Proceedings of the ASME 2019
International Design Engineering Technical Conferences
and Computers and Information in Engineering Conference
IDETC/CIE2019
August 18-21, 2019, Anaheim, CA, USA

DETC2019-98117

COORDINATED MODEL PREDICTIVE CONTROL ON MULTI-LANE ROADS

Nathan Goulet*
Clemson University International Center for
Automotive Research
Greenville, South Carolina
Email: ngoulet@clemson.edu

Beshah Ayalew
Clemson University International Center for
Automotive Research
Greenville, South Carolina
Email: beshah@clemson.edu

ABSTRACT

There are significant economic, environmental, energy, and other societal costs incurred by the road transportation sector. With the advent and penetration of connected and autonomous vehicles there are vast opportunities to optimize the control of individual vehicles for reducing energy consumption and increasing traffic flow. Model predictive control is a useful tool to achieve such goals, while accommodating ego-centric objectives typical of heterogeneous traffic and explicitly enforcing collision and other constraints. In this paper, we describe a multi-agent distributed maneuver planning and lane selection model predictive controller that includes an information sharing and coordination scheme. The energy saving potential of the proposed coordination scheme is then evaluated via large scale microscopic traffic simulations considering different penetration levels of connected and automated vehicles.

1 INTRODUCTION

In 2017, the transportation sector accounted for 29% of the total energy consumed by the United States, and 55% of that was used to power light-duty vehicles, including cars, small trucks, vans, sport-utility vehicles, and motorcycles [1]. This means that approximately 16% of all energy consumed in the United states goes towards personal transportation. With the advent of connected and automated vehicles (CAVs), there is great potential to optimize the velocity and acceleration profiles of vehicles in order to minimize the overall energy consumption. This is particularly important on multi-lane roads, as approximately one third of all vehicle miles traveled in the United States, between 2010 and 2015, were on multi-lane interstates or other freeways and highways [2]. To this end, this paper presents an information sharing and coordinated model predictive control (MPC) scheme for CAVs within mixed traffic of human-driven passenger vehicles and other CAVs on multi-lane roads.

We will begin by reviewing algorithms for lane decisions with individualized or selfish objectives. These fall into three categories: rule-, behavioral-, and optimization-based algorithms. Rule-based algorithms such as those described in [3–5], utilize a set of rules and a finite state machine in order to trigger a lane change when a given threshold is reached. These may be difficult to generalize and result in sub-optimal behavior due to the potentially arbitrary nature of the thresholds. The next group, behavioral methods, typically rely on machine-learning techniques in order to model the behavior of human drivers [6, 7]. Methods based on partially observable Markov decision processes (POMDP) can be computationally inefficient. However, there is ongoing research into creating efficient online algorithms [7]. The last category, optimization-based algorithms, may utilize search methods to find near optimal solutions, such as in [8], or numerical optimization via mixed integer programming (MIP) [9, 10] or non-linear programming (NLP) [11, 12] in a receding horizon manner. These methods are typically advantageous due to their ability to explicitly handle state and input constraints while optimizing performance with respect to some cost func-

*Address all correspondence to this author.

tion. Further, there is already extensive work present in multi-agent MPC [13, 14], which allows these methods to be expanded to multiple vehicles within a traffic environment.

The three categories of multi-agent MPC include centralized, decentralized, and distributed MPC. Centralized MPC consists of one central controller for all agents that results in optimal system performance. Unfortunately, centralized control quickly becomes intractable and computationally burdensome as the size of the system grows, and it is ineffective at handling faults, which is not ideal for safety critical systems [14]. Decentralized MPC breaks the large scale system into decoupled subsystems that each solve their own optimal control problem without knowledge of the actions of other subsystems. This technique reduces the computational burden for each subsystem, and is more flexible to changes in the system topology, however, performance can be significantly degraded with strong coupling between subsystems [13, 14]. Distributed MPC (DMPC) accounts for coupling between subsystems by communicating information about planned trajectories. This allows for a flexible and still scalable subsystem-based control structure while maintaining good performance in the presence of coupling between subsystems, making this an ideal approach for CAVs [13, 14].

DMPC strategies have been successfully implemented in other multi-agent system applications. For example, [15] presents and implements a DMPC strategy for unmanned aerial vehicles, which utilizes a safety cost that penalizes deviations in the plan transmitted to other agents in order to increase the predictability of agents. DMPC has also been successfully implemented within vehicular platoons, such as in [16] for longitudinal control while ensuring string stability. Lastly, [10] presents a coordinated MPC formulated as a MIP that controls longitudinal accelerations and commands a lane change based on tracking a desired velocity and minimizing accelerations, without explicitly considering coordination within the cost function.

This paper builds on the lane decision MPC presented in [11, 12], through addition of a sharing and coordination scheme in order to implement the controller as a distributed MPC. For the purposes of this paper, the communication between CAVs is assumed to be present through currently available technologies such as dedicated short range communication (DSRC) or cellular connections. In this work, we do not consider losses associated with these connections but they can be included in future investigations.

The structure of the remainder of the paper is as follows. Section 2 presents an overview of the control framework and sharing scheme; Sections 3-5 detail the modules of the framework (object vehicle prediction, reference speed assigner, and DMPC, respectively); Section 6 presents results and a discussion thereof; and Section 7 provides concluding remarks and potential future research. Throughout this paper, the phrases ego vehicle, and CAV i will be used interchangeably.

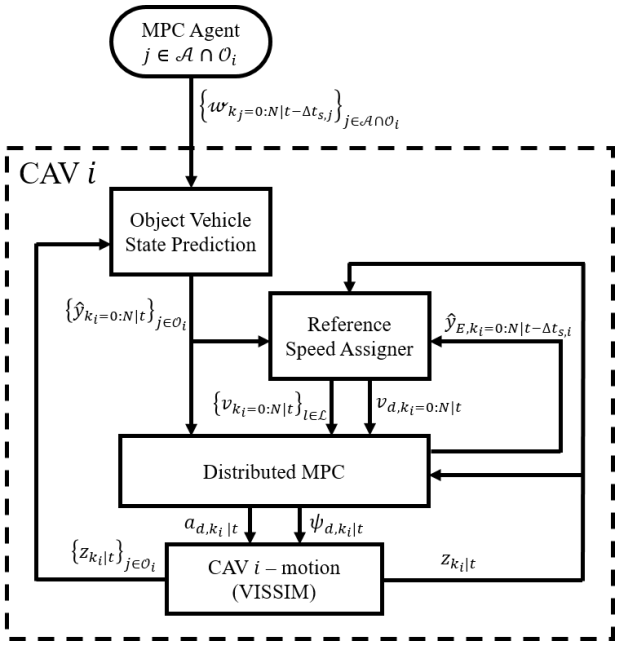

FIGURE 1. CONTROL FRAMEWORK FOR THE i^{th} CAV

2 CONTROL FRAMEWORK AND INFORMATION SHARING SCHEME

The control framework for a given CAV i in the group of CAVs $\mathcal{A}$ is presented in Fig. 1. At a given time t, it is assumed that CAV i acquires state measurements, $\{z_{k_i|t}\}_j$, of each object vehicle (OV) $j \in \mathcal{O}_i$, where $\mathcal{O}_i$ is the set of OVs within the neighborhood of CAV i, and k_i is the prediction time-step index of CAV i. These measurements are assumed to come from on-board sensors, or vehicle-to-vehicle (V2V) or vehicle-to-infrastructure (V2I) communication. Measurement uncertainties, data association and fusion of sensed and communicated state measurements are beyond the scope of this paper, however, interested readers may find a potential framework within [17].

The j^{th} OV may be in one of two subsets of $\mathcal{O}_i$, the neighboring CAVs where $j \in \mathcal{A} \cap \mathcal{O}_i$, or the neighboring human-driven OVs where $j \in \mathcal{O}_i \setminus \mathcal{A}$. Moving forward, the OVs will be referred to as CAV j or HD j, respectively. From each CAV j, CAV i receives a time-delayed plan via V2V communications in the form of an information matrix $\{w_{k_j=0:N|t-\Delta t_{s,j}}\}_j$, where $\Delta t_{s,j}$ is the information time delay from CAV j, and N is the number of steps in the prediction horizon. Fig. 2 presents a sample traffic scenario showing the communication link between three CAVs, therein the information matrix is represented as $\mathcal{W}_j$.

The object vehicle prediction block then predicts the trajectories of the HD j, assuming decoupled constant lateral velocity and constant longitudinal acceleration kinematics models. Whereas, for each CAV j the OV prediction module shifts and translates the shared plan, via linear interpolation between prediction time-steps, to the current measurement $\{z_{k_i|t}\}_j$ using the

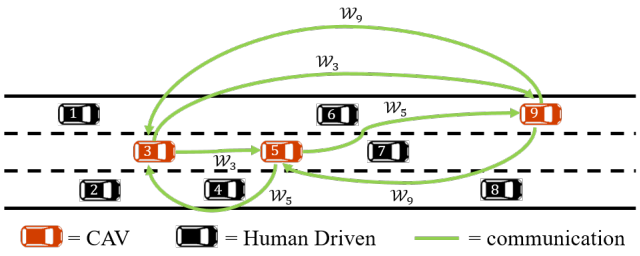

FIGURE 2. TRAFFIC ENVIRONMENT ILLUSTRATING INFORMATION SHARING

method in Sec. 3. The OV predicted output matrix $\{\hat{y}_{k_i=0:N|t}\}_j$ is then passed to the reference speed assigner and distributed MPC blocks for calculations of lane reference and desired velocities, and enforcing collision avoidance constraints, respectively.

The reference speed assigner block also takes in state measurements $z_{k_i|t}$ of CAV i from on-board sensors, and the prior predicted trajectory from the DMPC $\hat{y}_{k_i=0:N|t-\Delta t_{s,i}}$, where $\Delta t_{s,i}$ is the update rate of the MPC. With this information, a reference speed, $\{v_{k_i=0:N|t}\}_l$, is assigned to each lane $l \in \mathscr{L}$ over the prediction horizon according to a set of rules presented in Sec. 3.4, where $\mathscr{L}$ is the set of lanes on the current link. Concurrently, a desired speed, $v_{d,k_i=0:N|t}$, is set for CAV i. The DMPC then plans the optimal trajectory based on CAV i's desired speed, the lane reference speeds and the predicted states for each OV $j \in \mathscr{O}_i$. The DMPC block passes the desired longitudinal acceleration $a_{d,k_i|t}$ and deviation angle from the lane centerline $\psi_{d,k_i|t}$ from the first time-step within the prediction horizon to the lower level motion controller. Then, the process is repeated at the next MPC update.

3 Object Vehicle Prediction

3.1 Human-driven Object Vehicles

Due to the low computational cost, the HD j is modeled using decoupled constant velocity lateral and constant acceleration longitudinal kinematics, as presented in (1).

$$\hat{x}_{j,k_i+1|k_i} = \begin{bmatrix} 1 & \Delta t_{p,j} & \frac{1}{2}\Delta t_{p,j}^2 & 0 & 0 \\ 0 & 1 & \Delta t_{p,j} & 0 & 0 \\ 0 & 0 & 1 & 0 & 0 \\ 0 & 0 & 0 & 1 & \Delta t_{p,j} \\ 0 & 0 & 0 & 0 & 1 \end{bmatrix} \begin{bmatrix} s \\ v_s \\ a_s \\ y_e \\ v_{y_e} \end{bmatrix}_{j,k_i|k_i} \tag{1a}$$

$$\hat{y}_{j,k_i|k_i} = \begin{bmatrix} s \\ y_e \\ v_t \end{bmatrix}_{j,k_i|k_i}, \tag{1b}$$

The states of HD j are $\hat{x}_j = \begin{bmatrix} s & v_s & a_s & y_e & v_{y_e} \end{bmatrix}_j^T$, where s_j, $v_{s,j}$, and $a_{s,j}$ are the position, velocity and acceleration along the path of j, respectively, and $y_{e,j}$ and $v_{y_e,j}$ are the lateral deviation from centerline and lateral velocity of j, respectively. In (1), $\Delta t_{p,j}$ is the prediction time-step and $\hat{y}$ are the relevant outputs for the reference speed assigner and DMPC. The tangential velocity of OV j, $v_{t,j}$, is calculated as $v_{t,j,k_i|k_i} = \sqrt{v_{s,j,k_i|k_i}^2 + v_{y_e,j,k_i|k_i}^2}$.

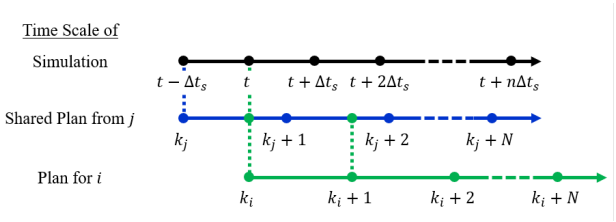

FIGURE 3. TIME SCALES FOR THE SIMULATION, CAV j, AND CAV i

There are unfortunately errors associated with these decoupled kinematic models, as vehicles are actually nonholonomic, dynamic systems, however, the relatively fast update rate of the DMPC mitigates some of the errors associated with this assumption.

3.2 Connected and Automated Object Vehicles

CAV j passes the information matrix $\{w_{k_j=0:N|t-\Delta t_{s,j}}\}_j$ to i with the following set $\{\hat{y}_{k_j=0:N}\ t-\Delta t_{s,j}\}_j$, where $\hat{y}_{k_j=0:N}$ is the output matrix of CAV j provided over the prediction horizon $k_j = 0:N$. In general, the time delay may not be equivalent to the size of a prediction horizon time-step Δt_p, as the update rate of the DMPC and frequency of communications may be faster. It is assumed that from the time the plan was made $t-\Delta t_{s,j}$ to the current time t, CAV j has followed its planned trajectory. For simplicity, it is assumed that the prediction time steps, prediction lengths, and control update and communication rates are equivalent for all CAVs, i.e. $\Delta t_{p,j} = \Delta t_{p,i} = \Delta t_p$, $N_j = N_i = N$, and $\Delta t_{s,j} = \Delta t_{s,i} = \Delta t_s$, respectively. Fig. 3 illustrates the differences in time.

Equation (2), presents the interpolation formula used to synchronize a given state ξ within the plan of CAV j from time-steps $k_j = 0:N-1|t-\Delta t_{s,j}$ to the current time-step of CAV i, $k_i = 0:N-1|t$.

$$\xi_{j,k_i} = z_{j,k_i|t} \quad for\ k_i = 1 \tag{2a}$$

$$\Delta\xi_{j,k_j} = \xi_{j,k_j+1} - \xi_{j,k_j} \tag{2b}$$

$$h_{k_j} = \sqrt{\Delta\xi_{j,k_j}^2 + \Delta t_p^2} \tag{2c}$$

$$\theta_{k_j} = \tan^{-1}\left(\frac{\Delta\xi_{j,k_j}}{\Delta t_p}\right) \tag{2d}$$

$$\xi_{j,o} = z_{j,k_i|t} - \frac{\Delta t_s}{\Delta t_p} h_1 \cos\theta_1 \tag{2e}$$

$$\xi_{j,k_i} = \tfrac{\Delta t_s}{\Delta t_p} h_{k_j} \cos\theta_{k_j} + \xi_{j,o} \quad for\ k_i = 2:N-1, \tag{2f}$$

where h_{k_j} and θ_{k_j} are the Euclidean distance traveled and direction of travel in the t-ξ plane by j from k_j to k_j+1, and $\xi_{j,o}$ is the translation term to move the start of the plan to the new measured position $z_{j,k_i|t}$. At time-step N of i, it is assumed the CAV j follows the same trajectory as it did from $k_j = N-1:N$.

4 Distributed Model Predictive Control Formulation

The MPC for a given agent $i \in \mathscr{A}$ is formulated in (3) below. In the remainder of this paper, k or the subscript k is in reference to the time discretization index k_i of CAV i.

$$\min_{\mathbf{u}_k} \sum_{k=1}^{N_p} \left[\|F_{l,k}\|^2_{P_f} + \|G_k\|^2_{P_g} \right] + \sum_{k=1}^{N_p-1} \left[\|H_k\|^2_{P_h} + \|u_k\|^2_R \right] \tag{3a}$$

$$\dot{x} = f(x,u), x \in X, u \in U \tag{3b}$$

$$c(x,u) \geq 0 \tag{3c}$$

The cost function (3a) comprises of the lane-dependent output tracking cost $F_{l,k}$, the lane-independent output tracking cost G_k, a predictability cost H_k, and $\mathbf{u}_k = \left[u_k, u_{k+1}, \cdots, u_{k+N}\right]^T$ is the control input trajectory over the prediction horizon. P_f, P_g, P_h, and R are the respective weighting matrices. Each term of the cost function will be discussed in further detail in the following subsections. Equation (3b) is the dynamics model of agent i, $\dot{x} = f(x,u)$, subject to the state and output constraints, $x \in X$ and $u \in U$, where X and U are the sets of all permissible states and control inputs, respectively. Finally, (3c) is the set of output constraints $c(x,u)$ detailed below.

4.1 Ego Motion Model

A non-linear particle motion model within a path intrinsic Frenet frame is used to describe the dynamics of a CAV utilizing the DMPC. The model is depicted in Fig. 4. The position along the lane centerline is s, y_e is the deviation from the lane centerline, v_t is the tangential velocity, ψ is the angle of the CAV relative to the tangent of the lane centerline, $\kappa(s)$ is the curvature of the lane as a function of s, and O_g, X_g, and Y_g are the origin, x-axis, and y-axis of the global frame, respectively. The equations governing the dynamics model are as follows [18]:

$$\dot{x} = \begin{bmatrix} \dot{s} \\ \dot{y}_e \\ \dot{v}_t \\ \dot{\psi} \\ \dot{a}_t \end{bmatrix} = \begin{bmatrix} v_t \left(\frac{1}{1-y_e\kappa(s)} \right) \cos\psi \\ v_t \sin\psi \\ a_t \\ -\tau_\psi \psi \\ -\tau_{a_t} a_t \end{bmatrix} + \begin{bmatrix} 0 & 0 \\ 0 & 0 \\ 0 & 0 \\ \tau_\psi & 0 \\ 0 & \tau_{a_t} \end{bmatrix} \begin{bmatrix} \psi_d \\ a_{t,d} \end{bmatrix}, \tag{4}$$

where a_t is the tangential acceleration, and both ψ and a_t are assumed to have first order dynamics with time constants τ_ψ and τ_{a_t}, and desired inputs ψ_d and $a_{t,d}$, respectively. The outputs $\hat{y}$ passed to the reference speed assigner are then $\hat{y} = \begin{bmatrix} s & y_e & v_t \end{bmatrix}^T$. A 4^{th}-order Runge-Kutta explicit integrator is used to descretize and solve the model in (4) within the MPC.

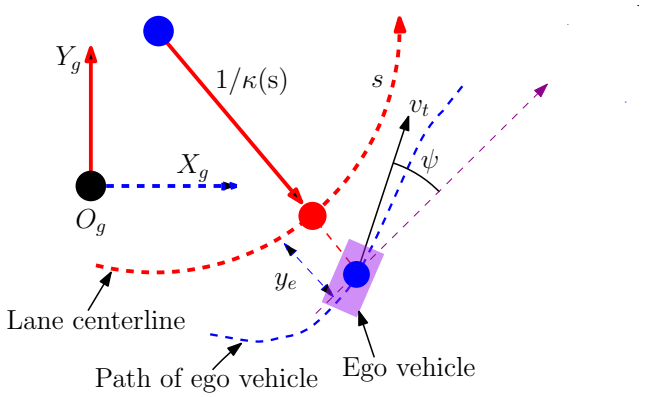

FIGURE 4. EGO VEHICLE MOTION IN THE FRENET FRAME

4.2 State, Input, and Output Constraints

The CAV states, inputs and outputs are subject to the following environmental, and physical limits:

$$\underline{y}_e \leq y_e \leq \overline{y}_e \tag{5a}$$

$$v_t \leq \overline{v}_t. \tag{5b}$$

$$\underline{a}_{t,d} \leq a_{t,d} \leq \overline{a}_{t,d} \tag{5c}$$

$$\underline{a}_{n,d} \leq v_t^2 \kappa(s) + v_t \dot{\psi} \leq \overline{a}_{n,d} \tag{5d}$$

where $\underline{y}_e$, $\overline{y}_e$, $\overline{v}_t$, $\underline{a}_{t,d}$, $\overline{a}_{t,d}$, $\underline{a}_{n,d}$, and $\overline{a}_{n,d}$ are the right roadway bound, left roadway bound, speed limit, tangential acceleration lower and upper limits, and normal acceleration lower and upper limits, respectively. For clarity the subscript k has been omitted in (5) and will be omitted for the remainder of this section; however, it should be noted that the constraints are evaluated at each step of the prediction horizon, unless otherwise mentioned.

The position of the CAV is also subject to collision avoidance constraints that are posed in (6) as a hyper-ellipse centered about the object vehicles position enlarged to account for both the size of the ego vehicle and OV j.

$$\left(\frac{y_{e,i} - y_{e,j}}{\Delta y_{ij}} \right)^4 + \left(\frac{s_i - s_j}{\Delta s_{ij} + a\zeta_{\Delta s}} \right)^4 \geq 1 \tag{6}$$

The axes of the hyper-ellipse in the s- and y_e-directions are Δy_{ij}, and Δs_{ij}, respectively. As presented in [18], both are determined based on a minimum safe distance, and outer dimensions of the ego vehicle and OV. The slack variable $\zeta_{\Delta s}$ is introduced as an

additional state, with the dynamics $\dot{\zeta}_{\Delta s} = u_{\zeta_{\Delta s}}$ and constraint $\zeta_{\Delta s} \geq 0$, where $u_{\zeta_{\Delta s}}$ is a decision variable. $\zeta_{\Delta s}$ ensures a comfortable following distance during normal driving, but allows for closer following in emergency situations. The coefficient a is a tuning parameter that determines the magnitude of the slack distance.

At the end of the prediction horizon the hyper-elliptical constraint is enlarged to ensure stability. As an example, the enlargement of the s-axis will be presented and it is noted that an analogous method may be used for the y_e-axis. The goal is to ensure that the ego vehicle can obtain a zero relative velocity with the OV beyond the prediction horizon before entering a collision state. By assuming decoupled constant acceleration kinematics for the ego vehicle and OV, the time t_{safe} required for the ego vehicle to obtain zero relative velocity is:

$$t_{safe} = \frac{v_{s,i} - v_{s,j}}{a_{s,j} - a_{s,i}}. \tag{7}$$

The acceleration of the ego vehicle $a_{s,i} \in \left\{\underline{a}_{s,i}, \overline{a}_{s,i}\right\}$ where $\underline{a}_{s,i}$ is the braking limit and $\overline{a}_{s,i}$ is the upper acceleration limit of CAV i. It can be seen from (7) that $\text{sign}\left(v_{s,i} - v_{s,j}\right) = -\text{sign}\left(a_{s,j} - a_{s,i}\right)$ for a positive safe time to obtain zero relative velocity, and $a_{s,i}$ is chosen accordingly. The safe distance, D_{safe}, required for the ego vehicle to obtain a zero relative velocity with OV j at the end of the prediction horizon is then:

$$D_{safe} = \left| \frac{\left(v_{s,i} - v_{s,j}\right)^2}{2\left(a_{s,j} - a_{s,i}\right)} \right|. \tag{8}$$

Therefore, the major axis at the end of the prediction horizon is $\Delta s_{ij,N} = \Delta s_{ij,N_o} + D_{safe}$, where $\Delta s_{ij,N_o}$ is the base size of the axis calculated as previously mentioned.

4.3 Cost Function

The four different terms of the cost function (3) (lane-dependent cost $F_{l,k}$, lane-independent cost G_k, predictability cost H_k, and input (energy) penalty) will be discussed in further detail here.

4.3.1 Lane-dependent Cost The lane-dependent cost is defined as follows:

$$F_{l,k} = \begin{bmatrix} d_{1,k}\left(y_e,k - y_{e,1,k}\right) \\ \vdots \\ d_{N_l,k}\left(y_{e,k} - y_{e,N_l,k}\right) \\ d_{1,k}\left(v_{t,k} - v_{1,k}\right) \\ \vdots \\ d_{N_l,k}\left(v_{t,k} - v_{N_l,k}\right) \end{bmatrix} \tag{9}$$

where $d_{l,k}$, with $l \in \{1,\ldots,N_l\}$, is a decision variable that is 1 when the CAV is choosing the lane l and zero otherwise. Further, $y_{e,l,k}$ is the position of the lane centerline relative to the road center, and $v_{l,k}$ is the reference velocity associated with the respective lane, which is assigned through rules described in Sec. 5. In order to solve the MPC as a non-linear program, instead of a mixed integer program, the lane decision variables have been relaxed [11, 12], with the following dynamics and constraints:

$$\dot{d}_{l,k} = u_{d_{l,k}} \quad \forall l \in \{1,\cdots,N_l - 1\} \tag{10a}$$

$$\sum_{l=1}^{N_l-1} d_{l,k} \leq 1 \quad \forall d_{l,k} \in [0,1] \tag{10b}$$

$$d_{N_l,k} = 1 - \sum_{l=1}^{N_l-1} d_{l,k}, \tag{10c}$$

where $u_{d_{l,k}}$ is the control variable for the respective lane. This results in a blending of the costs for tracking each lane. Say, for example, CAV i is tracking lane $l = 2$ well, without any error, then the minimum of (9) will occur with $d_2 = 1$ and $d_l = 0\ \forall l \neq 2$, so that the other non-zero lane tracking terms will drop out.

4.3.2 Lane-independent Cost The lane-independent cost is defined as follows:

$$G_k = \begin{bmatrix} v_{t,k} - v_{d,k} & \zeta_{\Delta s,k} - v_{t,k} & 1 - \sum_{l=1}^{N_l} d_{l,k}^2 \end{bmatrix}^T, \tag{11}$$

where $v_{d,k}$ is the desired velocity of CAV i. The first term in (11) is the desired velocity tracking term, the second term explicitly makes the collision avoidance slack variable, $\zeta_{\Delta s}$, velocity dependent, and the last term is utilized to help ensure the controller chooses one lane (eventually, at the optimum).

4.3.3 Predictability Cost The predictability cost is designed to penalize the CAV for deviating from its prior plan. The goal is to penalize unpredictable behaviour in order to mitigate oscillations due to adjacent CAVs recursively re-planning according to the shared plan of the other CAVs from the prior time-step. The predictability cost is formulated as:

$$H_k = \begin{bmatrix} s_k - s_{t^-,k} & y_{e,k} - y_{e,t^-,k} \end{bmatrix}^T, \tag{12}$$

where $s_{t^-,k}$ and $y_{e,t^-,k}$ are the shifted and translated position along the path and lateral deviation from the road centerline from the plan of CAV i at time-step $t - \Delta t_s$. A similar linear interpolation method as presented in Sec. 3 is used to shift and translate the planned trajectory of CAV i.

4.3.4 Input Cost The input cost term penalizes the control inputs over the prediction horizon, $u_k = \left[a_{t,d}\ \psi_d\ u_{\zeta_{\Delta s}}\ u_{d_1}\ \ldots\ u_{d_l}\right]^T$. The penalty on $a_{t,d}$ minimizes the longitudinal acceleration and is used to supplement a direct cost on energy. The cost on ψ_d may be tuned to obtain desired lateral dynamics when changing lanes, while the costs on $u_{d_1}\ \ldots\ u_{d_l}$ may be tuned to optimize lane decisions. Lastly, the penalty on $u_{\zeta_{\Delta s}}$ is present to guarantee there exists a unique solution to the optimal control problem.

5 Reference Speed Assigner

The reference speed assigner, adopted from [11], utilizes a set of rules to determine the reference speed of a given lane. Algorithm 1 outlines the rules that are applied for each OV j within each lane l at each step of the prediction horizon. Line 1 of the algorithm checks if the vehicle is within a distance of interaction based on $v_{t,k}$ and a time headway t_{int}. Then line 2 checks if the CAV is leading/following OV j, or if it is alongside OV j. If the result of line 2 is true, then line 3 checks if OV j is going below the speed limit. If OV j is travelling at a velocity less than the speed limit, then the lane reference speed is set to $v_{t,j,k}$, otherwise it is set to the speed limit. If the result of line 2 is false, then the lane reference speed is set to the base desired speed of the vehicle $v_{d_o,k}$. After each lane has a set reference speed the CAVs desired speed $v_{d,k}$ is updated to the lane reference speed that is closest to $v_{d_o,k}$, in order to mitigate choosing multiple lanes.

Algorithm 1 Lane reference speed assigner

1: **if** $(|s_k - s_{j,k}| < t_{int} v_{t,k})$ **then**
2: **if** $\left((s_k - s_{j,k})\ (v_{t,k} - v_{t,j,k}) < 0\right)$ **or** $\left(|s_k - s_{ov,k}| < \Delta s_{ij} + a\zeta_{\Delta s}\right)$ **then**
3: **if** $v_{t,j,k} < \bar{v}_{t,k}$ **then**
4: $v_{l,k} = v_{t,j,k}$
5: **else**
6: $v_{l,k} = \bar{v}_{t,k}$
7: **end if**
8: **else**
9: $v_{l,k} = v_{d_o,k}$
10: **end if**
11: **end if**

6 RESULTS AND DISCUSSION

Our coordinated DMPC scheme was implemented within the traffic micro-simulation software package VISSIM [19] using the external driver model utility. We used the ACADO toolkit and qpOASES solver [20] to solve the online optimization problem of the DMPC at each CAV. The traffic network consisted of a straight section of 3 lane one-way highway $\approx$ 3000m long.

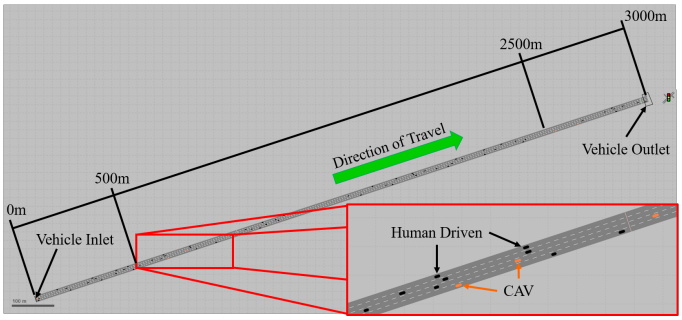

FIGURE 5. SNAPSHOT OF A SAMPLE* VISSIM SIMULATION; CAVs ARE ORANGE, AND HUMAN DRIVEN VEHICLES ARE BLACK (*Image shown has 4 lanes, while link utilized in simulation has 3 lanes)

The desired speed of vehicles was distributed about $\approx$ 86.5km/h (or 24m/s). The link had a prescribed vehicle flow rate of 2250 veh/hr or 750 veh/lane/hr. The relative portion (penetration) of CAVs in the flow was 0%, 25%, 50%, and 100%. The human driven object vehicles were simulated using the Wiedemann car following model and VISSIMs rule-based lane decision algorithm [19]. Fig. 5 shows a snapshot of the traffic network in VISSIM. Each simulation was run for approximately 10 minutes of traffic with vehicles freely entering and exiting the network at the inlet and outlet nodes.

In order to negate the impacts of transients associated with vehicles entering and exiting the network, fuel and travel time calculations were performed on data from 500m to 2500m, omitting the first and last 500m. Additionally, to allow the network to reach a steady state at the prescribed veh/hr flow rate, vehicles that entered the network prior to the first vehicle exiting were ignored in fuel and travel time calculations. Further, vehicles that did not reach 2500m before the simulation ended were also omitted. In all 135 vehicles were evaluated for each of the 10 minute simulations. Fuel calculations were made using the methods and engine specifications from [21].

As a baseline for evaluating the performance of the proposed control framework, we will define the desired fuel consumption rate as follows: the desired fuel consumption is the fuel consumption required to maintain a constant velocity (with 0 accelerations) equal to the vehicles desired velocity v_{d_o}. Similarly we will define the desired travel time as the time required for a given vehicle to traverse the link while maintaining a constant velocity equal to v_{d_o}.

Figure 6 presents the percentage change in observed average fuel consumption relative to the average desired fuel consumption. At all tested CAV penetrations (25%, 50% and 100%), the fleet (HDs and CAVs combined) outperformed the 0% penetration scenario. This resulted in a 4% reduction in fuel consumed at 25% CAV penetration when compared to 0% CAV penetration. Similarly, there is respectively, a 5.2% and 7% reduction

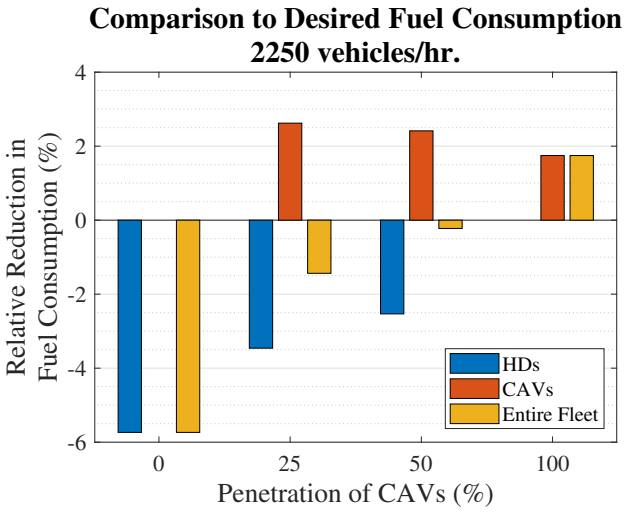

FIGURE 6. REDUCTION IN FUEL CONSUMPTION AT 0%, 25%, 50%, AND 100% CAV PENETRATION RELATIVE TO DESIRED.

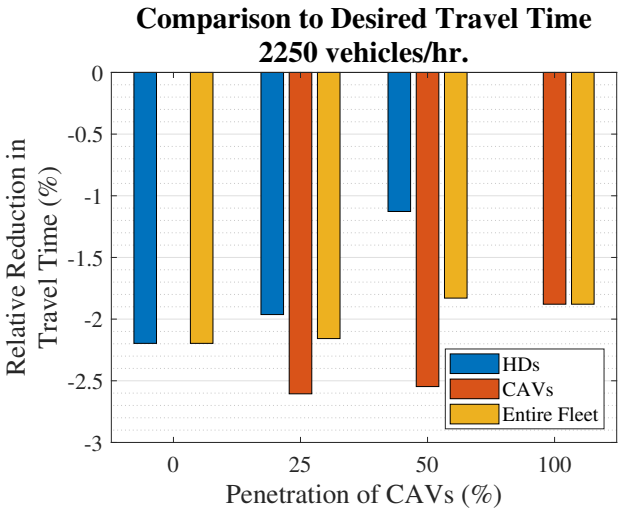

FIGURE 7. REDUCTION IN TRAVEL TIME AT 25% AND 50% CAV PENETRATION RELATIVE TO 0% PENETRATION.

in the fuel consumed by the fleet at 50% and 100% CAV penetration relative to 0% CAV penetration. The gains did come at a nominal cost to the CAVs, which had a higher increase in travel time relative to desired when compared to the HDs, as seen in Fig. 7. Despite the longer travel times for CAVs the average travel time for the fleet did reduce in Fig. 7 at 25% and 50% CAV penetration, as the HDs traveled faster through the link.

It should be noted that the CAVs actually outperform the desired case when it comes to fuel consumption in Fig. 6. When CAV penetration increases, the CAVs are able to track their desired velocities more closely (noted by the improved travel time relative to desired in Fig. 7) and the reduction in fuel consumption of CAVs relative to the baseline decreases in Fig. 6. This makes the trade-off between travel time and fuel consumption evident. As the controller is currently designed to track an arbitrarily prescribed desired velocity, there is opportunity to further improve fuel consumption by either developing an optimized reference speed assigner based on desired arrival times, or by reformulating the DMPC to track a desired arrival time instead of a desired velocity.

7 CONCLUSION

An information sharing and coordination scheme was developed in order to implement the multi-lane maneuver planning algorithm presented in [12] in a coordinated and distributed manner on multiple CAVs. When implemented within the traffic micro-simulation software VISSIM, the coordinated distributed control scheme shows promise for decreasing energy consumption, however, more extensive and exhaustive scenarios with higher traffic volumes, higher CAV penetrations, and a more complex network, as well as a statistically relevant sample size, is required to better understand the impact of the distributed MPC. Additionally, as noted in Section 6, there may be possible further fuel consumption gains realized by reformulating the DMPC to track a desired arrival time instead of a desired velocity or by prescribing an optimized reference velocity trajectory.

Further gains may be realized by incorporating a shared cost, or a common goal to optimize the reference velocity of CAVs for improved traffic flow and a reduction in energy consumption, while still meeting travel time requirements. Additional future work will include accounting for measurement noise, communication losses, and disturbances in order to make the coordinated distributed control scheme robust to such uncertainties, as they were not considered here. There are also significant issues with object vehicle prediction: the kinematics models result in large errors further into the prediction horizon. The development of a computationally efficient prediction model that accounts for interactions between other OVs, the ego vehicle, and the traffic network (e.g. stop signs, traffic signals, changes in speed limits, etc.) is another avenue for further research.

ACKNOWLEDGMENT

This research was supported by an award from the U.S. Department of Energy Vehicle Technologies Office (Project No. DE-EE0008232)

REFERENCES

[1] U.S. Energy Information Adminstration, 2018. Use of Energy in the United States Explained: Energy Use for Transportation.

[2] U.S. Department of Transportation Federal Highway Administration Policy and Governmental Affairs Office of Highway Policy Information, 2016. Annual Vehicle-Miles of Travel, 1980-2015 By Functional System: National Summary.

[3] Gipps, P., 1986. "A model for the structure of lane-changing decisions". *Transportation Research Part B: Methodological,* ***20***(5), oct, pp. 403–414. doi: 10.1016/0191-2615(86)90012-3.

[4] Kesting, A., Treiber, M., and Helbing, D., 2007. "General Lane-Changing Model MOBIL for Car-Following Models". *Transportation Research Record: Journal of the Transportation Research Board,* ***1999***, pp. 86–94. doi: 10.3141/1999-10.

[5] Wang, Q., Weiskircher, T., and Ayalew, B., 2015. "Hierarchical Hybrid Predictive Control of an Autonomous Road Vehicle". In Proceedings of the ASME 2015 Dynamic System and Control Conference, ASME, p. V003T50A006. doi: 10.1115/DSCC2015-9773.

[6] Tehrani, H., Do, Q. H., Egawa, M., Muto, K., Yoneda, K., and Mita, S., 2015. "General behavior and motion model for automated lane change". In 2015 IEEE Intelligent Vehicles Symposium (IV), no. Iv, IEEE, pp. 1154–1159. doi: 10.1109/IVS.2015.7225839.

[7] Ulbrich, S., and Maurer, M., 2013. "Probabilistic online POMDP decision making for lane changes in fully automated driving". In 16th International IEEE Conference on Intelligent Transportation Systems (ITSC 2013), no. Itsc, IEEE, pp. 2063–2067. doi: 10.1109/ITSC.2013.6728533.

[8] Berntorp, K., and Cairano, S. D., 2016. "Joint decision making and motion planning for road vehicles using particle filtering". *IFAC-PapersOnLine,* ***49***(11), pp. 175 – 181. 8th IFAC Symposium on Advances in Automotive Control AAC 2016.

[9] Du, Y., Wang, Y., and Chan, C. Y., 2014. "Autonomous lane-change controller via mixed logical dynamical". *2014 17th IEEE International Conference on Intelligent Transportation Systems, ITSC 2014*, pp. 1154–1159. doi: 10.1109/ITSC.2014.6957843.

[10] Dollar, R. A., and Vahidi, A., 2018. "Predictively Coordinated Vehicle Acceleration and Lane Selection Using Mixed Integer Programming". In Proceedings of the ASME 2018 Dynamic Systems and Control Conference, ASME, p. V001T09A006. doi: 10.1115/DSCC2018-9177.

[11] Wang, Q., Ayalew, B., and Weiskircher, T., 2016. "Optimal assigner decisions in a hybrid predictive control of an autonomous vehicle in public traffic". In 2016 American Control Conference (ACC), Vol. 2016-July, IEEE, pp. 3468–3473. doi: 10.1109/ACC.2016.7525450.

[12] Wang, Q., Ayalew, B., and Weiskircher, T., 2019. "Predictive maneuver planning for an autonomous vehicle in public highway traffic". *IEEE Transactions on Intelligent Transportation Systems,* ***20***(4), April, pp. 1303–1315. doi: 10.1109/TITS.2018.2848472.

[13] Scattolini, R., 2009. "Architectures for distributed and hierarchical Model Predictive Control – A review". *Journal of Process Control,* ***19***(5), may, pp. 723–731. doi: 10.1016/j.jprocont.2009.02.003.

[14] Li, S., and Zheng, Y., 2017. *Distributed Model Predictive Control for Plant-Wide Systems*. John Wiley & Sons, Incorporated,.

[15] Bertrand, S., Marzat, J., Piet-Lahanier, H., Kahn, A., and Rochefort, Y., 2014. "MPC Strategies for Cooperative Guidance of Autonomous Vehicles". *AerospaceLab*(8), pp. 1–18.

[16] Dunbar, W. B., and Caveney, D. S., 2012. "Distributed Receding Horizon Control of Vehicle Platoons: Stability and String Stability". *IEEE Transactions on Automatic Control,* ***57***(3), mar, pp. 620–633. doi: 10.1109/TAC.2011.2159651.

[17] Yoon, D. D., Nawaz Ali, G. M., and Ayalew, B. "Data Association and Fusion Framework for Decentralized Multi-Vehicle Cooperative Perception". In Proceedings of the ASME 2019 International Design Engineering Technical Conferences & Computers and Information in Engineering Conference (IDETC 2019), (IDETC2019-98001). August 18-21, 2019. Anaheim, CA, USA. .

[18] Weiskircher, T., Wang, Q., and Ayalew, B., 2017. "Predictive guidance and control framework for (semi-) autonomous vehicles in public traffic". *IEEE Transactions on Control Systems Technology,* ***25***(6), Nov, pp. 2034–2046. doi:10.1109/TCST.2016.2642164.

[19] Group, PTV, 2018. PTV Vissim 10 User Manual.

[20] Houska, B., Ferreau, H., and Diehl, M., 2011. "ACADO Toolkit – An Open Source Framework for Automatic Control and Dynamic Optimization". *Optimal Control Applications and Methods,* ***32***(3), pp. 298–312.

[21] Dollar, R. A., and Vahidi, A., 2017. "Quantifying the impact of limited information and control robustness on connected automated platoons". In 2017 IEEE 20th International Conference on Intelligent Transportation Systems (ITSC), pp. 1–7. doi: 10.1109/ITSC.2017.8317604.